

The Hydrogen Equation of State at High Densities

J. Vorberger and D.O. Gericke

*Centre for Fusion, Space and Astrophysics, Department of Physics,
University of Warwick, Coventry CV4 7AL, United Kingdom**

W.-D. Kraeft

Institut für Physik, Universität Rostock, 18051 Rostock, Germany

We use a two-fluid model combining the quantum Green's function technique for the electrons and a classical HNC description for the ions to calculate the high-density equation of state of hydrogen. This approach allows us to describe fully ionized plasmas of any electron degeneracy and any ionic coupling strength which are important for the modelling of a variety of astrophysical objects and inertial confinement fusion targets. We have also performed density functional molecular dynamics simulations (DFT-MD) and show that the data obtained agree with our approach in the high density limit. Good agreement is also found between DFT-MD and quantum Monte Carlo simulations. The thermodynamic properties of dense hydrogen can thus be obtained for the entire density range using only calculations in the physical picture.

PACS numbers: 52.25.Dg, 52.25.Kn, 52.27.Gr

Keywords: dense plasmas, equation of state, *ab initio* simulations

I. INTRODUCTION

The properties of a variety of astrophysical objects are essentially determined by the high-density equation of state (EOS) of hydrogen^{1,2}. Hydrogen is fully ionized at these high densities independent of the temperature. In this metallic phase, the electrons can be of arbitrary degeneracy including the highly degenerate limit ($T=0$) and the ions are strongly coupled. The thermodynamics is thus strongly influenced by the well-pronounced short-range order in the proton subsystem although the major contributions stem from the electron gas.

Metallic hydrogen occurs in the interior of giant gas planets like Jupiter, Saturn and similar extrasolar planets^{1,3,4}. The temperatures encountered along the isentrope of giant planets are in the order of a few electron volts. At densities comparable to solids and above, a $T=0$ description of the electrons is possible for colder planets, whereas temperature related corrections might be needed for hotter planets⁵. Higher temperatures and densities are found in white dwarf stars and the crust of neutron stars^{6,7}. As most elements are fully ionized under these conditions, matter behaves hydrogen-like and the EOS is again determined by a combination of degenerate electrons and strongly coupled ions.

Beyond astrophysical applications, the EOS of dense hydrogen is also required to model inertial confinement fusion experiments as the compression path of the fuel runs through the parameter space considered here^{8,9}. Although at much higher densities, the fully compressed DT-pellet has similar properties when considering electron degeneracy and ionic coupling strength.

Most astrophysical objects exhibit an isentrope that covers several phases. For example the internal structure of giant gas planets is determined by phase transitions as the molecular to metallic or atomic to metallic transition in dense fluid hydrogen (sometimes named plasma phase

transition^{10,11}). After many investigations leaving the nature of this transition unclear¹²⁻²⁰, recent first principle simulations showed that a first order phase transition with surprisingly small volume change is indeed likely^{21,22}.

However, present *ab initio* simulations like DFT-MD, path integral Monte Carlo (PIMC), or coupled electron-ion Monte Carlo (CEIMC) cover a limited parameter space only. For a consistent description of the EOS, one has to require that i) different techniques agree in overlapping regions and ii) the simulation data merge with well-founded theories in limiting cases. The second point has been achieved only in the low density region where PIMC simulations match density and fugacity expansions of the EOS perfectly²³.

In this paper, we focus on the high-density limit of the equation of state of fluid hydrogen. As quantum Monte Carlo schemes are not available for very high densities, we rely on DFT-MD simulations here. However, first principle simulations like DFT-MD have so far been unable to provide results that converge into the high density, i.e. Gell-Mann & Brueckner, $T=0$ limit. We resolve this issue by carefully performed DFT-MD simulations for higher densities and by employing an analytic approach that extends the $T=0$ limiting law to parameters with finite temperatures. We can then demonstrate agreement in overlapping regions of density, so that the goal of a combined EOS of hydrogen, that is solely based on methods in the physical picture and covers the entire density range for temperatures of a few electron volts, is reached.

The analytic EOS theory we apply for high densities is a two-fluid model based on a perturbation with respect to the electron-ion interaction. It keeps all contributions from correlations in the ion subsystem and is applicable for arbitrary degeneracy of the electrons. Thus, our two-fluid model is valid for fully ionized plas-

mas with, compared to thermal energies and/or ion-ion interactions, weak electron-ion interactions.

After an introduction of the model in the next section, we present results and comparisons with data from first principle quantum simulations. In particular, we show which steps are necessary to reach agreement between our two-fluid model and the simulations and also give limits for the applicability of both.

II. ANALYTICAL EOS APPROACH

We consider fully ionized plasmas consisting of protons and electrons. To characterize the interaction strength between the particles, we define the classical coupling parameter

$$\Gamma = \frac{e^2}{dk_B T} \quad \text{with} \quad d = \left(\frac{4\pi}{3} n \right)^{-1/3}. \quad (1)$$

In the quantum regime, the classical kinetic energy scale has to be replaced by its quantum analog: $k_B T \rightarrow \frac{2}{3} \langle K_a \rangle$. The mean kinetic energy $\langle K_a \rangle$ can be calculated via a Fermi integral²⁵ which recovers both the classical as well as the fully degenerate (Fermi energy) limits. Note that *classically* all coupling parameters are identical for hydrogen while the electron-electron and the electron-ion coupling are strongly reduced in plasmas with highly degenerate electrons as $\langle K_e \rangle \gg k_B T$ holds here. In the quantum limit, the electron coupling parameter Γ_e becomes smaller than unity due to quantum degeneracy. Here, the Brueckner parameter $r_s = d/a_B$ is commonly used to describe the coupling strength.

A. Two-Fluid Model

For the parameters considered here, the electron-proton interactions are weak ($\Gamma_{ei} \ll 1$) while the proton-proton coupling is usually strong ($\Gamma_{ii} \geq 1$). The weak interactions between electrons and protons allows us to apply a Born-Oppenheimer approximation and treat the electrons in linear response to the fields created by the ions. As a result, one can rewrite the full two-component problem as a one-component system for the ions which interact via effective potentials. More precisely, this will be called the two-fluid model where the fully correlated electron and ion fluids interact only weakly with each other. Of course, this procedure eliminates the ability to describe bound states which is however unnecessary in the high density limit. Applying this two-fluid model, the pressure is given by^{26,27}

$$\frac{\beta p}{n_i} = 1 + \frac{\beta}{V} \frac{dF(n_i)}{dn_i} - \frac{1}{2} \beta n_i \int d\mathbf{r} [g_{ii}(r) - 1] \left(\frac{r}{3} \frac{\partial}{\partial r} - n_i \frac{\partial}{\partial n_i} \right) v_{ii}^{\text{eff}}(r). \quad (2)$$

with

$$F = F_{eg} + \frac{N_i}{2} \int \frac{d\mathbf{k}}{(2\pi)^3} v_{ei}^2(k) \chi_{ee}(k). \quad (3)$$

A similar model was also used by, e.g., Chabrier & Potekhin^{28,29}. The first term in Eq. (2) represents the ideal contribution from the classical ions. In the second term, the density derivative of the free energy F produces the contribution of the correlated electron gas via the free energy of the isolated electron subsystem F_{eg} . The integral over the electron density response function χ_{ee} , to be taken in random phase approximation (RPA), is an electron-ion cross term that arises from the linear response treatment of the electrons in the two-fluid description. The third term in Eq. (2) accounts for ionic correlations described by the pair distribution g_{ii} . The polarizability of the electron gas is here to be taken into account via an effective ion-ion potential v_{ii}^{eff} . This potential must also be applied when calculating the ionic pair distribution. The density derivative arises as the effective ion-ion potential is density dependent via the screening function.

The internal energy can be calculated similarly via

$$\frac{\beta U}{V} = \frac{3}{2} n_i + \frac{\beta}{V} U_0(n_i) + \frac{1}{2} \beta n_i^2 \int d\mathbf{r} [g_{ii}(r) - 1] \left[v_{ii}^{\text{eff}}(r) - T \frac{\partial}{\partial T} v_{ii}^{\text{eff}}(r) \right]. \quad (4)$$

Again, we have first the ideal ion contribution and U_0 denotes the internal energy of the electron subsystem. It may be approximated by the free energy F (3) for highly degenerate systems near $T = 0$; otherwise it is given by $U_0 = F - T \partial F / \partial T$. Ionic correlations are accounted for by the integral term. The additional temperature derivative is due to the fact that the effective ion-ion potential is also temperature-dependent.

B. Properties of the Ion Subsystem

The effective ion-ion interaction consistent with the model above is given by

$$v_{ii}^{\text{eff}}(k) = v_{ii}(k) + [v_{ei}(k)]^2 \chi_{ee}(k), = \frac{4\pi e^2}{k^2} \varepsilon_e^{-1}(k). \quad (5)$$

Here, the electron part in the static dielectric function in RPA, $\varepsilon_e^{-1} = 1 + v_{ee} \chi_{ee}$, was introduced. $v_{ee} = 4\pi e^2 / k^2$ is the Coulomb potential between electrons²⁵. The bare Coulomb interaction between the protons v_{ii} is thus linearly screened by the electrons. More simple approximations for the effective potential can be obtained for small k , where the Debye or Yukawa potential, $v_{ii}^{\text{eff}}(k) = 4\pi e^2 / (k^2 + \kappa_e^2)$ with $\kappa_e^2 = (4e^2 m_e / \pi \hbar^3) \int_0^\infty dp f_e(p)$, follows.

The derivation of the two-fluid description (2) and (4) clearly shows that the ionic pair distribution g_{ii} must be

obtained from a one-component description of the ions where the forces are given by the effective interaction v_{ii}^{eff} . Possible methods to determine g_{ii} are classical Monte Carlo and molecular dynamics simulations or techniques based on integral equations like the hypernetted chain equations (HNC)^{30–35}.

C. Contributions of the Electron Gas

To describe the electron gas, we employ the quantum statistical method of thermodynamic Green's functions^{25,36}. Its advantage is the ability to describe systems with arbitrary temperatures including the correct $T = 0$ physics, the transition to Boltzmann statistics, and the correct high temperature (Debye-Hückel) law. Using this technique, a perturbation expansion in the interaction strength can be established^{23,25}. Including terms up to the second order, one obtains

$$p_{ee}(T_e, \mu_e) = p_e^{\text{id}}(T_e, \mu_e) + p_e^{\text{HF}}(T_e, \mu_e) + p_{ee}^{\text{MW}}(T_e, \mu_e) + p_e^{e^4 n}(T_e, \mu_e). \quad (6)$$

The terms are the ideal gas law, the Hartree-Fock (HF) quantum exchange term, the direct Montroll-Ward (MW) term, and quantum exchange contributions of the second order ($e^4 n$), respectively. As this perturbation expansion exists in the grand canonical ensemble, the density n_e is related to the chemical potential μ_e via

$$n_e(T_e, \mu_e) = \frac{\partial p_{ee}}{\partial \mu_e}. \quad (7)$$

An inversion within *golden rule* is performed in order to obtain the pressure as function of density²³. This means that correlation contributions of the free energy as function of density are taken to be equal to the negative excess pressure as function of the chemical potential.

The ideal pressure is given by

$$p_e^{\text{id}}(T_e, \mu_e) = \frac{2k_B T_e}{\Lambda_e^3} I_{3/2}(\mu_e/k_B T_e). \quad (8)$$

Here, $\Lambda_e = \sqrt{2\pi\hbar^2/m_e k_B T_e}$ is the thermal deBroglie wavelength and $I_{3/2}$ is the Fermi integral of order $3/2$ ²⁵.

First order exchange contributions are contained in the HF term

$$p_e^{\text{HF}}(T_e, \mu_e) = \frac{(2\sigma_e + 1)e^2}{\Lambda_e^4} \int_{-\infty}^{\mu_e/k_B T_e} d\alpha I_{-1/2}^2(\alpha), \quad (9)$$

which is given by an integral over a Fermi integral of the order $-1/2$.

The Montroll-Ward term can be computed by a double integral over the dielectric function of the electron gas ε_e

$$p_e^{\text{MW}}(T_e, \mu_e) = \frac{-1}{4\pi^3} \int_0^\infty dp p^2 \mathcal{P} \int_{\pm 0}^\infty d\omega \coth\left(\frac{\omega}{2k_B T_e}\right) \times \left[\arctan \frac{\text{Im}\varepsilon_e(p, \omega)}{\text{Re}\varepsilon_e(p, \omega)} - \text{Im}\varepsilon_e(p, \omega) \right]. \quad (10)$$

It is consistent with the expansion (6) to use the RPA dielectric function ε_e .

The normal e^4 exchange term, accounting for exchange effects of second order, can be written as an integral over Fermi functions, $f_p = [\exp(\beta p^2/2m_e - \beta\mu_e) + 1]^{-1}$, and Pauli-blocking factors, defined by $\bar{f}_p = [1 - f_p]$,

$$p_e^{e^4 n}(T_e, \mu_e) = m_e \int \frac{d\mathbf{p} d\mathbf{q}_1 d\mathbf{q}_2}{(2\pi)^9} v_{ee}(p) v_{ee}(\mathbf{p} + \mathbf{q}_1 + \mathbf{q}_2) \times \frac{f_{q_1} f_{q_2} \bar{f}_{\mathbf{q}_1 + \mathbf{p}} \bar{f}_{\mathbf{q}_2 + \mathbf{p}} - f_{\mathbf{q}_1 + \mathbf{p}} f_{\mathbf{q}_2 + \mathbf{p}} \bar{f}_{q_1} \bar{f}_{q_2}}{q_1^2 + q_2^2 - (\mathbf{p} + \mathbf{q}_1)^2 - (\mathbf{p} + \mathbf{q}_2)^2}. \quad (11)$$

Here, v_{ee} is the bare electron-electron Coulomb potential.

The expansion (6) accounts for direct correlations and dynamic screening, incorporates collective oscillations (plasmons) as well as quantum diffraction and exchange in the electron subsystem. This expression is valid for weakly coupled electrons of arbitrary degeneracy and includes in particular the low and high temperature limiting cases of Debye-Hückel and Gell-Mann & Brueckner, respectively²³.

Within the same quantum approach, protons can be incorporated and an EOS for hydrogen can be calculated²³. The advantage of an EOS of hydrogen fully based on Green's functions is its capability to describe quantum effects in the proton subsystem correctly. However, a hydrogen EOS based on expansion (6) is restricted to weak coupling in the proton subsystem as well, a limitation avoided within the two-fluid approach presented here.

D. Limiting Behavior and Applicability

The condition of weak electron-ion coupling as used to derive Eqs. (2) and (4) is fulfilled not only for the high density limit of highly degenerate electrons and strongly coupled ions, but also in the high temperature and low density limits. Here, all interactions are weak and of the same order and the EOS is given by the Debye-Hückel law²⁵

$$\beta p = \beta p^{\text{id}} + \beta p^{\text{DH}} = \sum_a n_a - \frac{\kappa^3}{24\pi}. \quad (12)$$

The first term is the ideal classical gas contribution, the second term is the Debye-Hückel correction determined by the total inverse screening length $\kappa^2 = \sum_a 4\pi Z_a e_a n_a \beta$. The sums in Eq.(12) and in the definition of κ run over all species $a = \{e, i\}$.

This limiting law is not fully reached by our two-fluid model. However, it deviates only by a tiny fraction of $p^{\text{DH}}/p^{2\text{-fluid}} = 16\sqrt{2}/23 = 0.99$ (similar for the internal energy and other thermodynamic functions). The slight disagreement can be traced back to the neglect of the influence of the ions on the electrons. Note that this result can only be obtained if the contributions of the electron gas are evaluated for finite temperatures and not just in the ground state.

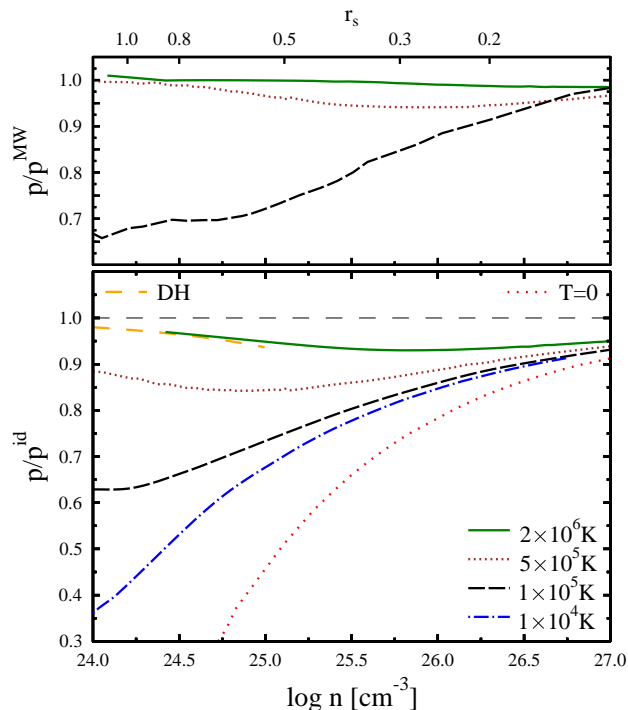


FIG. 1: (Color online) Lower panel: pressure of hydrogen as predicted by the two-fluid model (2) normalized by the ideal contribution. The high temperature (Debye-Hückel - DH) and high density ($T=0$) limits are given for comparison. Upper panel: ratio of the two-fluid model and the quantum statistical perturbation theory using the Montroll-Ward approximation for hydrogen^{23,25}.

Our quantum treatment via thermodynamic Green's functions also ensures that the electron contribution reaches the correct high density $T = 0$ limit. Moreover, the electron contribution is the by far largest term in the thermodynamic functions for high densities. Thus, the two-fluid model also recovers the high density $T = 0$ limit (with an error given by the ratio of electron to ion mass).

Consequently, the two-fluid model constitutes a valid approximation to the EOS of fully ionized and weakly coupled hydrogen plasmas with arbitrarily degenerate electrons. Both conditions are fulfilled for temperatures above $T = 2.5 \times 10^5$ K in the entire density range, where bound states do not occur and the coupling is sufficiently weak for the entire density range.

E. Results of the Two-Fluid Model

Figure 1 gives a general overview of the high-density EOS of hydrogen as calculated within the two-fluid model. Due to the normalization by the ideal pressure, the lines all approach unity for very high densities where the pressure is also independent of the temperature. At intermediate densities, the correlations yield a reduction

compared to the ideal pressure. These correlations can result from the occurrence of bound states or occur between free particles. Bound states can be excluded for the two highest temperatures in Fig. 1. Still, the improved description of ion-ion correlations within the two-fluid model yields a 10% correction compared to a description of the hydrogen EOS based entirely on Green's function theory.

The two-fluid model of Potekhin & Chabrier gives almost identical results to our approach in the parameter range where such a description can be expected to be valid, i.e. for metallic hydrogen and the high temperature low density case³⁷. This is a nontrivial finding as the electron theories used in this paper and by Potekhin & Chabrier are quite different.

In the case of the Green's function EOS^{23,25}, the correct high-density limit is an intrinsic feature related to the quantum treatment of both electrons and ions. In the two-fluid model, only the electrons are treated fully quantum statistically. Still, the two fluid system shows a similar behavior as the high density limit is dominated by the electron contribution. This fact holds although the ion-ion correlations strongly increases with density since the electron terms grow significantly faster. In addition, this behavior also minimizes the importance of the partition function of the strongly correlated ion fluid. For instance, small differences between Monte Carlo and HNC treatment of the ions at $\Gamma_{ii} = 130$ give a deviation of 2% in the ion system which will change the result of the total equation of state by 0.16%.

The approach to the exact high temperature limit (here given by the Montroll-Ward approximation of the Green's function theory) is demonstrated in the upper panel of Fig. 1. The two-fluid model can reproduce the exact law within 1% for $T = 2 \times 10^6$ K. The essential ingredient to achieve this result is the finite temperature description of the electrons. Moreover, it shows that the neglected influence of the ions on the electrons is very weak.

III. DFT-MD SIMULATIONS

DFT-MD simulations are a well-suited technique for the description of metallic hydrogen as it is encountered for example in the inner regions of giant gas planets. So far, there has been no overlap between an EOS calculated by DFT-MD and the correct $T = 0$ high-density models. To close this gap and to allow for a direct comparison of first principle DFT-MD simulations to our two-fluid model, we carried out DFT-MD calculations for very high densities which require special adjustments.

We used the DFT-MD programs VASP, CPMD, and abinit³⁸⁻⁴³. The number of electrons and protons in the simulations was $N = 128 \dots 432$. The temperature of the protons was controlled by a Nosé-Hoover thermostat⁴⁴. The time step in the MD simulation was chosen to be $\Delta t = 8$ a.u. = 0.194 fs. Every run covers at least 2 ps

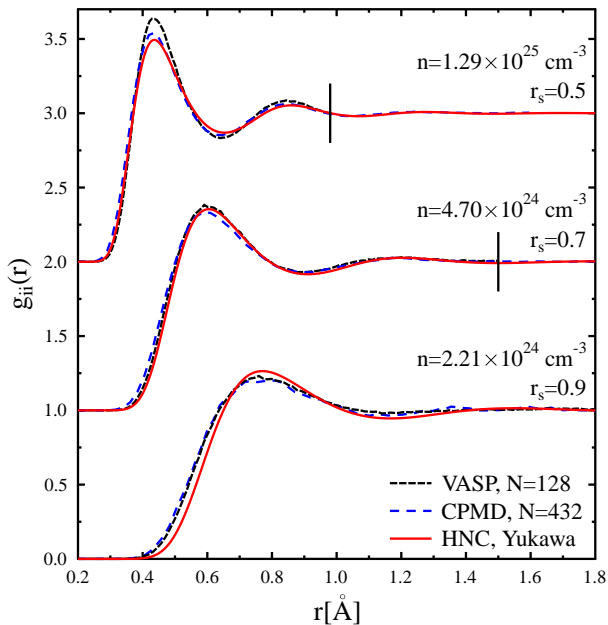


FIG. 2: (Color Online) Proton-proton pair distributions in hydrogen at a temperature of $T=10^4$ K for three different densities. Results of VASP (black dashed), CPMD (blue dashed, long spaces) and HNC using a linearly screened Yukawa potential (red solid) are compared. The black vertical lines indicate half the box length for the VASP runs. The lines for $r_s = 0.5$ and $r_s = 0.7$ have been shifted along the y-axis to improve readability.

after an initial equilibration. The exchange correlation functional was of Perdew-Burke-Ernzerhof type⁴⁵.

In VASP runs, the electron-ion pseudopotential was the standard (hard) projector augmented wave (PAW) potential as provided with the package^{46,47} and used here with a plane wave cutoff of 35 Ha. For densities higher than $n = 2.2 \times 10^{24} \text{ cm}^{-3}$ ($r_s \leq 0.9$), this was found to be too soft. Accordingly, a new harder GGA norm conserving local pseudopotential was generated using the optimized pseudopotential method as included in the Opium package⁴⁸. This new potential was then used in the CPMD code. It has a cutoff radius of $r_c = 0.5 a_B$ ($q_c = 15$, 6 Bessel functions) and requires a plane wave cutoff of 100 Ha to yield convergent results⁶⁶.

MD runs were usually performed using only Γ -point sampling of the Brillouin zone. Corrections due to k-point sampling can become important in the metallic region of hydrogen. Here, contributions of at most 2% were determined at randomly chosen snapshots where the pressure was reevaluated using $2 \times 2 \times 2$ and $4 \times 4 \times 4$ Monkhorst-Pack grids of k-points in abinit⁴⁹. Effects due to finite electron temperatures (Fermi smearing) have not been found for the high densities needed to achieve overlapping with the analytical theory.

As a first comparison between properties of our two-fluid model and *ab initio* DFT-MD simulations, Fig. 2 shows ion-ion pair distributions. The results using VASP

and CPMD deviate due to differences in the number of particles considered and the type of pseudopotential used. In the present study, all VASP runs have been performed with 128 electrons and 432 electrons were used in CPMD simulations. In addition, the CPMD runs use a much harder electron-ion pseudopotential having a core radius of $r_c = 0.5 a_B$ whereas $r_c = 0.8 a_B$ is used in the VASP runs. For the densities with $r_s = 0.9$ and $r_s = 0.7$, these differences are insignificant. However, both the harder pseudopotential and the increase in the number of particles / box size are important for the highest density with $r_s = 0.5$. Here, VASP predicts a first correlation peak that is too high which can be traced back to the too large core radius of the pseudopotential. Furthermore, a box with 128 particles is too small to allow for the computation of the structure at larger distances as it is seen in the tail of the pair distribution.

The pair distribution functions obtained from solutions of the hypernetted chain equations (HNC) are consistent with the approximations made to derive the two-fluid model. The HNC solver uses a linearly screened ion-ion potential and keeps the nonlinear correlations within the ion subsystem only. The comparison with the DFT-MD results shows that this is an appropriate model for the high densities shown (note that better agreement is obtained with the CPMD data for $r_s = 0.5$). Here, the electron-ion coupling strength is sufficiently low to justify the linear response formalism. For the lowest density with $r_s = 0.9$, there is some deviation in the first slope and in the strength of correlation that are a result of the linear screening approximation used. The comparison with the DFT-MD data demonstrate that the model of linear screening is beyond its limit of applicability for this density.

IV. RESULTS FOR THE EOS

We have already established that our two-fluid model merges with the exact $T = 0$ limiting law at the high density site of the EOS. In the following, we will show that this model and improved DFT-MD simulations give results in agreement with each other over a range of densities and temperatures. As DFT-MD and further Quantum Monte Carlo simulations already meet the exact low density limit (Debye-Hückel or density/fugacity expansions), the entire density range can now be described by theories in the physical picture.

Figure 3 and Table I include a comparison of EOS data obtained by the different simulation techniques. CEIMC results were taken from recent work²⁴. Unlike earlier CEIMC results⁵⁰, they give almost identical values for the pressure as obtained from DFT-MD. The data points span almost an order of magnitude in density and cover the region of metallic hydrogen which is most difficult to describe. This excellent agreement gives large confidence in both first principle simulations. As both data sets have a similar slope, we can expect that either both or none

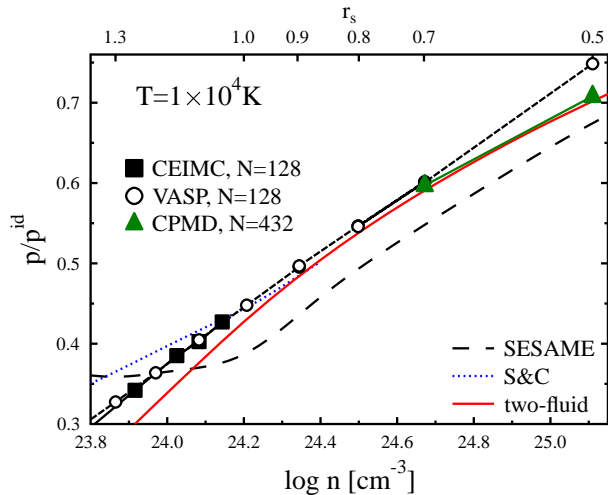


FIG. 3: (Color Online) Ratio of pressure to ideal pressure in hydrogen at $T = 10^4$ K versus density. Data shown are obtained using VASP¹⁷, VASP¹⁹ up to $r_s = 0.8$, CEIMC²⁴, Saumon & Chabrier EOS^{51,52}, and SESAME⁶³. The two-fluid model uses an effective ion-ion potential in RPA.

merge with the high-density description of the two-fluid model.

Figure 3 also shows a comparison of data obtained by *ab initio* simulations and results of the two-fluid model. At the low density side where CEIMC data exist, one finds considerable deviations. These differences are due to the decoupling of electrons and ions in the two-fluid EOS which is not applicable here.

To test the merging of the simulation data into the two-fluid description, we have to consider higher densities where the electron-ion coupling is weaker. For this task, we turn to DFT-MD simulations. In the case of VASP, this is not straightforward as one is not free in the choice of the electron-ion pseudopotential. Particularly, for densities above $r_s = 0.7$, the particles are closer together than the core radius of the pseudopotential. As we have already shown for the ion-ion pair distribution (see Fig. 2), this causes VASP to yield unreliable results for $r_s \leq 0.7$. As a result, the pressure obtained from VASP first approaches the results of the two-fluid model and then starts to deviate again for high densities.

The behavior of the VASP data demonstrates the need for a harder pseudopotential with a smaller core radius. Moreover, finite size effects become important for higher densities with larger correlation lengths. Both issues have been resolved in CPMD runs using a new pseudopotential with a core radius of $r_c = 0.5 a_B$ and $N = 432$ electrons and protons. The result show a smooth merging with the two-fluid model at high densities.

Figure 3 shows also results from EOS models often used in planetary modelling namely the SESAME tables and the EOS model constructed by Saumon & Chabrier⁵¹. The latter perfectly merges into our two-fluid model, but deviates from the quantum simulations

TABLE I: Comparison of the hydrogen EOS as obtained by VASP^{17,19}, CEIMC²⁴, CPMD (this work, using an improved electron-proton pseudopotential) and the two-fluid model (last two columns) using two effective proton-proton potentials as indicated.

r_s	3500 K	p/p^{id}				
	p^{id} [GPa]	VASP	CPMD	CEIMC	RPA	Hulthén
1.20	2.125e3	0.321	-	-	0.272	0.303
1.15	2.624e3	-	-	0.341	0.302	0.329
1.10	3.272e3	0.369	-	0.368	0.332	0.359
1.05	4.122e3	-	-	0.393	0.362	0.388
1.00	5.253e3	0.419	-	-	0.395	0.418
0.90	8.870e3	0.472	-	-	0.451	0.472
0.70	3.101e4	-	0.584	-	0.575	0.588
0.50	1.659e5	-	0.702	-	0.696	0.71

r_s	10^4 K	p/p^{id}				
	p^{id} [GPa]	VASP	CPMD	CEIMC	RPA	Hulthén
1.20	2.212e3	0.364	-	-	0.326	0.363
1.15	2.721e3	-	-	0.385	0.348	0.384
1.10	3.380e3	0.405	-	0.403	0.377	0.404
1.05	4.247e3	-	-	0.427	0.405	0.425
1.00	5.400e3	0.448	0.453	-	0.431	0.447
0.90	9.060e3	0.497	0.497	-	0.486	0.495
0.80	1.623e4	0.547	-	-	0.538	0.547
0.70	3.141e4	0.602	0.597	-	0.589	0.602
0.50	1.671e5	0.749	0.708	-	0.700	0.713

r_s	2×10^4 K	p/p^{id}				
	p^{id} [GPa]	VASP	CPMD	CEIMC	RPA	Hulthén
1.20	2.357e3	0.412	-	-	0.384	0.403
1.10	3.568e3	0.445	-	-	0.423	0.440
1.00	5.641e3	0.481	-	-	0.466	0.481
0.90	9.396e3	0.522	-	-	0.510	0.523
0.80	1.666e4	0.571	-	-	0.557	0.570
0.70	3.208e4	0.619	0.614	-	0.607	0.619
0.50	1.687e5	0.761	0.717	-	0.710	0.722

at lower densities. The SESAME data, on the other hand, disagree with both *ab initio* simulations and the two-fluid model over the whole density range considered.

V. EXTENSION AND DISCUSSION

A. Nonlinear Electron-Ion Interactions

A limitation of the two-fluid model arises from the use of first order perturbation theory to describe the response of the electrons to the fields created by the ions. One can however argue that the good agreement of the two-fluid model and the fully nonlinear simulations is a result of the fact that quadratic response terms cancel to a large extent⁵³.

An improved treatment including the fully nonlin-

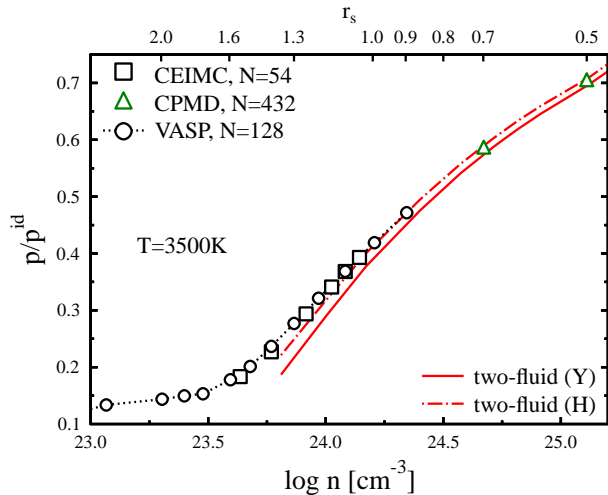


FIG. 4: (Color Online) Pressure of dense hydrogen at $T = 3500$ K normalized by the ideal pressure. The symbols mark simulation data similar to Fig. 3 (CEIMC data are interpolated for this temperature). The two curves show results of the two-fluid model with different ion-ion potentials: the linearly screened Yukawa potential (solid, red line) and the nonlinear Hulthén potential (red, dash-dotted line).

ear response (see, e.g., Refs.^{54–56}) is beyond the scope of this paper. Here, we estimate nonlinear effects in the electron-ion interaction by applying the nonlinear Hulthén potential⁵⁷

$$v_{ii}^{\text{H}}(r) = \frac{e^2 \kappa_e}{e^{\kappa_e r} - 1} \quad (13)$$

as an ad-hoc model for the effective ion-ion interaction.

Interestingly, the results of the two-fluid model agree rather well with the data from the quantum simulations for 3500K in Fig.4 if this nonlinear potential is used. In the density range with $1.1 \leq r_s < 0.7$, the agreement is much better than for the case of the linearly screened Yukawa potential. Indeed, Potekhin & Chabrier include local field corrections in the screening for the effective electron-proton interaction³⁷. For the parameters of Fig.4, our curve using the Hulthén potential and the curve according to their model are indistinguishable. However, there is no effect due to nonlinear electron-ion interactions for temperatures above 5000K and densities larger than $r_s = 0.9$.

B. Quantum Effects in the Ion Subsystem

For the highest densities considered, quantum effects may also become important for the ions. To estimate quantum effects on the protons, we first consider a potential that accounts for quantum diffraction effects of

order e^{258}

$$v_{ii}^{\text{KK}}(r) = \frac{Z^2 e^2 \sqrt{\pi}}{2 \lambda_i \kappa_e r} \left\{ \exp\left(-\kappa_e r + \frac{\lambda_i^2 \kappa_e^2}{4}\right) \times \left[\Phi\left(\frac{r}{\lambda_i} - \frac{\lambda_i \kappa_e}{2}\right) + 2\Phi\left(\frac{\lambda_i \kappa_e}{2}\right) - 1 \right] + \exp\left(\kappa_e r + \frac{\lambda_i^2 \kappa_e^2}{4}\right) \left[1 - \Phi\left(\frac{r}{\lambda_i} + \frac{\lambda_i \kappa_e}{2}\right) \right] \right\}. \quad (14)$$

Here, κ_e is the inverse screening length of the electrons, $\lambda_i = \sqrt{\hbar/(2m_{ii}k_B T)}$ is the thermal wavelength of the ions with the reduced ion mass $m_{ii} = m_i/2$, and $\Phi(x)$ denotes the error function⁵⁹. For large distances, the quantum potential (14) approaches the screened effective ion-ion potential (5). At the origin, it has the finite value

$$\lim_{r \rightarrow 0} v_{ii}^{\text{KK}} = \frac{Z^2 e^2 \sqrt{\pi}}{\lambda_i} \exp\left(\frac{\lambda_i^2 \kappa_e^2}{2}\right) \left[1 - \Phi\left(\frac{\lambda_i \kappa_e}{2}\right) \right], \quad (15)$$

which reflects quantum diffraction effects.

Moreover, quantum exchange effects can be important for high densities. These can be included by adding the following exchange potential⁶⁰

$$v_{ii}^{\text{ex}}(r) = \frac{1}{2} \exp(-r^2/\lambda_i^2) \times \left[k_B T - \frac{Z^2 e^2 \pi}{4r} \int_0^1 \frac{d\alpha}{\alpha} \Phi\left(\frac{r\alpha}{\lambda_i \sqrt{1-\alpha}}\right) \right]. \quad (16)$$

The first term accounts for ideal exchange in an averaged way whereas the second term gives the e^2 contribution.

The quantum potentials (14) and (16) are derived from Slater sums, and are exact in the sense of perturbation theory. They give the correct quantum thermodynamic functions in the weakly coupled and weakly degenerate limit, i.e., for systems with $\Gamma_{ii} \ll 1$ and $n\Lambda_i^3 = n(2\pi\hbar/m_i k_B T)^{3/2} \ll 1$. We use these potentials here to estimate for which densities quantum effects start to influence the ion properties. It should be emphasized that the quantum potentials (14) and (16) are used *only* in the classical method employed to determine the pair distribution function g_{ii} (here, in the HNC solver). The thermodynamic expressions (2) and (4) are valid in quantum as well as in the classical case. Hence, the effective ion-ion potential (5) must be used without any quantum corrections in these formulas.

Figure 5 shows ion pair distributions obtained using the usual screened potential (5) and the quantum pseudopotential. Deviations become obvious for plasmas with $n\Lambda_i^3 > 0.6$. It can be observed that the quantum effects weaken the short range order in the proton system. It is however remarkable that these effects only set in at these high values of degeneracy. The reason for this behavior is found in the strong Coulomb forces at high densities that create a large correlation hole. Consequently, the protons are too far apart to experience short range diffraction and quantum exchange effects.

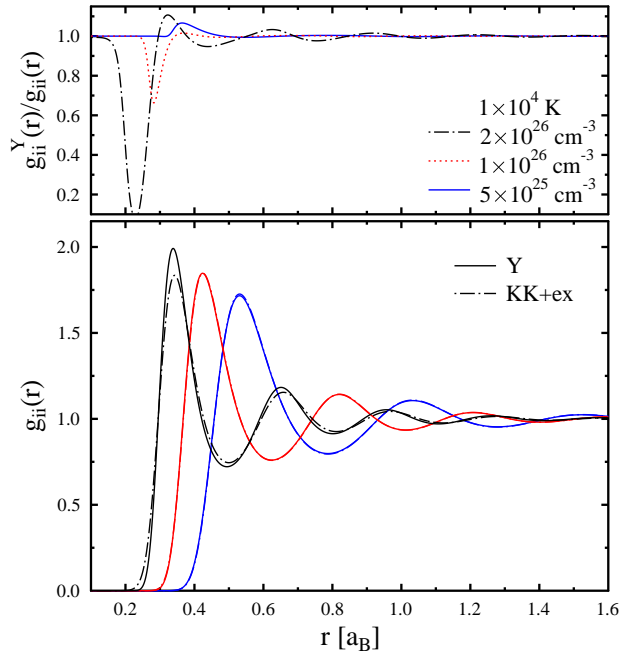


FIG. 5: (Color Online) Ion-ion pair distributions for $T=10^4$ K and three densities calculated by HNC using the screened potential (5) (solid lines, labelled Y) and the screened quantum potential with exchange (14) plus (16) (dash-dotted lines, KK+ex). The ion degeneracy is $n\Lambda_i^3 = 0.26, 0.52, 1.05$ for the three densities, respectively. The ion-ion coupling is $\Gamma_{ii} = 99(96), 125(119), 157(144)$, respectively, where the quantum coupling strength is given in brackets. The upper panel gives the ratio of the pair distributions with and without quantum effects.

The emerging quantum effects in the ion structure yield only small changes in the ion contribution to the thermodynamic functions. We determine a reduction of less than 1% in the correlation contribution to the ion pressure for plasmas with $n\Lambda_i^3 \leq 1$. At higher densities, the deviations from the classical result can be large, but their exact calculation requires PIMC methods.

The only quantum effect outside our control are zero point oscillations of the ions. In strongly coupled liquids, caging of the ions occurs and, for the time the cage is stable, the ions perform oscillations as in a solid⁶¹. PIMC calculations in the solid and fluid phases of a Yukawa system did indeed find contributions due to the zero point motion, but for very high densities of $n = 10^{27} \text{ cm}^{-3}$ ⁶². Moreover, the overall change in energy due to quantum oscillations is below 1% for the parameters considered. Furthermore, DFT-MD simulations, that do not include quantum oscillations of the ions, and CEIMC results, that include them, agree well in the considered parameter range which again indicates that these effects are small.

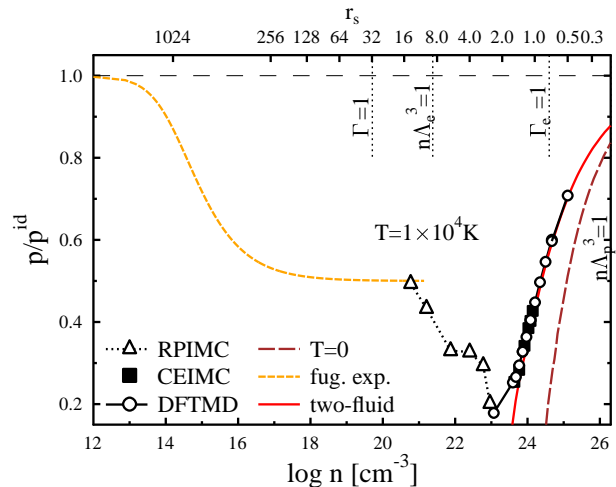


FIG. 6: (Color Online) Pressure over ideal pressure of a hydrogen plasma with $T=10^4$ K for a wide density range covering the ideal classical plasma state, the atomic gas, the molecular gas, and the metallic fluid (from left to right). The lines show the fugacity expansion from Ref.²⁵, the two-fluid model (this work) using an effective ion-ion potential in RPA, and the $T=0$ limit. The symbols mark simulation data from RPIMC⁶⁴, CEIMC²⁴, and DFT-MD from this work and Refs.^{17,19}.

C. Hydrogen EOS for Arbitrary Densities

The two-fluid model, based on the quantum statistical Green's function approach for the electron contributions and classical HNC methods for the ion properties, is well applicable in the density range that is neither covered by present first principle simulations nor by the $T=0$ limit. After examining the high-density part of the EOS in detail, it is worth noting that theories and simulations in the physical picture can be used to cover the entire parameter range *and* show agreement in overlapping regions of their applicability.

Figure 6 demonstrates this fact for an isotherm that covers the low density ideal plasma, the atomic fluid, the molecular fluid, and the metallic fluid to the border of the fully degenerate electron-proton system. Although each phase requires well-suited theories or simulations, one finds a smooth EOS that is often based on several methods and that does not involve any interpolation. Such a combined EOS can serve as an excellent basis for the modelling of gas planets and other compact objects dominated by hydrogen.

VI. CONCLUSIONS

We have applied a two-fluid model to investigate the hydrogen EOS at high densities. Our approach combines the advantages of a quantum theory based on thermodynamic Green's functions for the electrons with a classical

description of the structure in the ion fluid. Thus, it is able to account for electron degeneracy, finite temperatures, and strong forces between the ions. Its only limitation is the requirement of weak electron-ion interactions which naturally excludes bound states.

The two-fluid model agrees very well with a number of exact limiting laws: i) at low densities it almost exactly merges with the Debye-Hückel law; ii) at high energies it practically coincides with the $T = 0$ limit as long as quantum effects on the proton subsystem are negligible; and iii) for high plasma temperatures it agrees with a perturbation expansion in terms of interaction strength for the entire density range.

In the high density region, we find excellent agreement of the two fluid model with first principle simulations (DFT-MD). Our DFT-MD simulations agree also well with recent CEIMC results. At lower densities ($r_s > 0.7$), the request of weak electron-ion coupling is not fulfilled and one finds increasing deviations between the results of the two-fluid model and the quantum simulations. For densities with $r_s \leq 0.7$, the two-fluid model is however a reliable and computationally cheap alternative to full scale quantum simulations. From the agreement in pressure and ion structure between simulations and two-fluid model, we can conclude that the exchange correlation functional used in DFT-MD and our Green's function approach give the same electronic contributions for the

relevant parameters. The two-fluid model also bridges the parameter space where neither DFT-MD simulations nor the $T = 0$ law can be applied. This success means that hydrogen can confidently be described in large parts of the phase diagram by techniques using the physical picture. For temperatures of a few electron volts relevant for astrophysics and inertial fusion, this includes the entire density range.

Although the two-fluid model was applied here only for hydrogen, it is also applicable for any fully ionized system with higher ion charge states or very stable inner shell configurations with small modifications. The essential test is if the electron-ion interaction can be considered to be small. Accordingly, systems like the fluid region in white dwarfs can be confidently described by the two-fluid model presented here as well.

Acknowledgement

The authors are grateful to B. Holst, W. Lorenzen, and R. Redmer for valuable remarks and comparisons with their DFT-MD results. We also thank M. Schlanges for stimulating discussions. Financial support from the UK's Engineering and Physical Sciences Research Council is gratefully acknowledged.

* Electronic address: j.vorberger@warwick.ac.uk

¹ T. Guillot, *Annu. Rev. Earth Planet. Sci.* **33**, 493 (2005).

² J.J. Fortney, S.H. Glenzer, M. Koenig, B. Militzer, D. Saumon, D. Valencia, *Phys. Plasma* **16**, 041003 (2009).

³ B. Militzer, W.B. Hubbard, J. Vorberger, I. Tamblyn, S.A. Bonev, *Astrophys. J.* **688**, L45 (2008).

⁴ N. Nettelmann, B. Holst, A. Kietzmann, M. French, R. Redmer, D. Blaschke, *Astrophys. J.* **683**, 1217 (2008).

⁵ A. Burrows *et al.*, *Astrophys. J.* **491**, 856 (1997).

⁶ P. Dufour *et al.*, *Nature* **450**, 522 (2007).

⁷ D. Saumon, S.B. Jacobson, *Astrophys. J.* **511**, L107 (1999).

⁸ J.D. Lindl *et al.*, *Phys. Plasmas* **11**, 339 (2004).

⁹ S.X. Hu, B. Militzer, V.N. Goncharov, S. Skupsky, *Phys. Rev. Lett.* **104**, 235003 (2010).

¹⁰ G.E. Norman, A.N. Starostin, *High Temp.* **6**, 394 (1968).

¹¹ G.E. Norman, A.N. Starostin, *High Temp.* **8**, 381 (1970).

¹² S.T. Weir, A.C. Mitchell, W.J. Nellis, *Phys. Rev. Lett.* **76**, 1860 (1996).

¹³ D. Beule, W. Ebeling, A. Förster, H. Juranek, S. Nagel, R. Redmer, G. Röpke, *Phys. Rev. B* **59**, 14177 (1999) and references therein.

¹⁴ S. Scandolo, *PNAS* **100**, 3051 (2003).

¹⁵ K.T. Delaney, C. Pierleoni, D.M. Ceperley, *Phys. Rev. Lett.* **97**, 235702 (2006).

¹⁶ B. Jakob, P.-G. Reinhard, C. Toepffer, G. Zwirnagel, *Phys. Rev. E* **76**, 036406 (2007).

¹⁷ J. Vorberger, I. Tamblyn, B. Militzer, S.A. Bonev, *Phys. Rev. B* **75**, 024206 (2007).

¹⁸ V.E. Fortov *et al.*, *Phys. Rev. Lett.* **99**, 185001 (2007).

¹⁹ B. Holst, R. Redmer, M.P. Desjarlais, *Phys. Rev. B* **77**, 184201 (2008).

²⁰ I. Tamblyn, S.A. Bonev, *Phys. Rev. Lett.* **104**, 065702 (2010).

²¹ M.A. Morales, C. Pierleoni, E. Schwegler, D.M. Ceperley, *PNAS* **107**, 12799 (2010).

²² W. Lorenzen, B. Holst, R. Redmer, *Phys. Rev. B* **82**, 195107 (2010).

²³ J. Vorberger, M. Schlanges, W.-D. Kraeft, *Phys. Rev. E* **69**, 046407 (2004).

²⁴ M.A. Morales, C. Pierleoni, D.M. Ceperley, *Phys. Rev. E* **81**, 021202 (2010).

²⁵ D. Kremp, M. Schlanges, W.-D. Kraeft, *Quantum Statistics of Nonideal Plasmas* Springer (Berlin), (2005).

²⁶ N.W. Ashcroft, D. Stroud, *Sol. State Phys.* **33**, 1 (1978).

²⁷ J.P. Hansen, I.R. McDonald, *Theory of Simple Liquids* Academix (London), (1986)

²⁸ G. Chabrier, *Phys. Lett. A*, **134**, 375 (1989).

²⁹ G. Chabrier, A.Y. Potekhin, *Phys. Rev. E* **58**, 4941 (1998).

³⁰ M.P. Allen, D.J. Tildesley, *Computer Simulation of Liquids*, Oxford Univ. Press (Oxford) (1987).

³¹ J.F. Springer, M.A. Pokrant, F.A. Stevens, *J. Chem. Phys.* **58**, 4863 (1973).

³² K. Ng, *J. Chem. Phys.* **61**, 2680 (1974).

³³ V. Schwarz *et al.*, *High Energy Density Phys.* **6**, 305 (2010).

³⁴ K. Wünsch, P. Hilse, M. Schlanges, D.O. Gericke, *Phys. Rev. E* **77**, 056404 (2008).

³⁵ K. Wünsch, J. Vorberger, D.O. Gericke, *Phys. Rev. E* **79**, 010201(R) (2009).

- ³⁶ W.-D. Kraeft, W. Kremp, W. Ebeling, G. Röpke, *Quantum Statistics of Charged Particle Systems* Akademie Verlag (Berlin), (1986).
- ³⁷ A.Y. Potekhin, G. Chabrier, *Contrib. Plasma Phys.* **50**, 82 (2010) and references therein, see <http://www.ioffe.ru/astro/EIP/> for the code.
- ³⁸ G. Kresse, J. Hafner, *Phys. Rev. B* **47**, 558 (1993).
- ³⁹ G. Kresse, J. Hafner, *Phys. Rev. B* **49**, 14251 (1994).
- ⁴⁰ G. Kresse, J. Furthmüller, *Phys. Rev. B* **54**, 11169 (1996).
- ⁴¹ CPMD, <http://www.cpmd.org/>, Copyright IBM Corp 1990-2008, Copyright MPI für Festkörperforschung Stuttgart 1997-2001.
- ⁴² X. Gonze *et al.*, *Computational Materials Science* **25**, 478 (2002).
- ⁴³ X. Gonze *et al.*, *Zeit. Kristallogr.* **220**, 558-562 (2005).
- ⁴⁴ W.G. Hoover, *Phys. Rev. A* **31**, 1695 (1985).
- ⁴⁵ J. P. Perdew, K. Burke, M. Ernzerhof, *Phys. Rev. Lett.* **77**, 3865 (1996).
- ⁴⁶ P. E. Blöchl, *Phys. Rev. B* **50**, 17953 (1994).
- ⁴⁷ G. Kresse and D. Joubert, *Phys. Rev. B* **59**, 1758 (1999).
- ⁴⁸ I. Grinberg, N.J. Ramer, A.M. Rappe, *Phys. Rev. B* **62**, 2311 (2000) and references therein.
- ⁴⁹ H.J. Monkhorst, J.D. Pack, *Phys. Rev. B* **13**, 5188 (1976).
- ⁵⁰ C. Pierleoni, D.M. Ceperley, M. Holzmann, *Phys. Rev. Lett.* **93**, 146402 (2004).
- ⁵¹ D. Saumon, G. Chabrier, H.M. van Horn, *Astrophys. J. Suppl.* **99**, 713 (1995).
- ⁵² D. Saumon, T. Guillot, *Astrophys J.* **609**, 1170J (2004).
- ⁵³ A.A. Louis, N.W. Ashcroft, *Phys. Rev. Lett.* **81**, 4456 (1998).
- ⁵⁴ R. Cenni, P. Saracco, *Nucl. Phys. A* **487**, 279 (1988).
- ⁵⁵ C.F. Richardson, N.W. Ashcroft, *Phys. Rev. B* **50**, 8170 (1994).
- ⁵⁶ S. Gravel, N.W. Ashcroft, *Phys. Rev. B* **76**, 144103 (2007).
- ⁵⁷ Y.P. Varshni, *Phys. Rev. A* **41**, 4682 (1990).
- ⁵⁸ Yu.L. Klimontovich, W.-D. Kraeft, *Theo. Phys. Math. Phys.* **19**, 364 (1974).
- ⁵⁹ M. Abramowitz, I.A. Stegun, *Handbook of Mathematical Functions* Dover (New York), (1972)
- ⁶⁰ W.-D. Kraeft, J. Vorberger, D.O. Gericke, M. Schlanges, *Contrib. Plasma Phys.* **47**, 253 (2007).
- ⁶¹ Z. Donko, G.J. Kalman, K.I. Golden, *Phys. Rev. Lett.* **88**, 225001 (2002).
- ⁶² B. Militzer, R.L. Graham, *J. Phys. Chem. Solids* **67**, 2136 (2006).
- ⁶³ S.P. Lyon, J.D. Johnson, eds. *Los Alamos National Laboratory EOS Database* (1992), Report LA-UR-92-3407, Table Hydr5251.
- ⁶⁴ B. Militzer, D.M. Ceperley, *Phys. Rev. E* **63**, 066404 (2001).
- ⁶⁵ V. Recoules, F. Lambert, A. Decoster, B. Canaud, J. Clerouin, *Phys. Rev. Lett.* **102**, 075002 (2009).
- ⁶⁶ A very hard pseudopotential is also used in Ref.⁶⁵, although with a capped energy-cutoff.